LungTrack: towards contactless and zero dead-zone respiration monitoring with commodity RFIDs

Lili Chen, Jie Xiong, Xiaojiang Chen, Sunghoon Ivan Lee, Daqing Zhang, Tao Yan, Dingyi Fang

LungTrack: Towards Contactless and Zero Dead-Zone Respiration Monitoring with Commodity RFIDs

LILI CHEN, Northwest University, International Joint Research Centre for Battery-free IoT, China
JIE XIONG, University of Massachusetts Amherst, USA
XIAOJIANG CHEN*, Northwest University, International Joint Research Centre for Battery-free IoT, China
SUNGHOON IVAN LEE, University of Massachusetts Amherst, USA
DAQING ZHANG, Télécom SudPais, France
TAO YAN, Northwest University, International Joint Research Centre for Battery-free IoT, China
DINGYI FANG, Northwest University, International Joint Research Centre for Battery-free IoT, China

Respiration rate sensing plays a critical role in elderly care and patient monitoring. The latest research has explored the possibility of employing Wi-Fi signals for respiration sensing without attaching a device to the target. A critical issue with these solutions includes that good monitoring performance could only be achieved at certain locations within the sensing range, while the performance could be quite poor at other "dead zones." In addition, due to the contactless nature, it is challenging to monitor multiple targets simultaneously as the reflected signals are often mixed together. In this work, we present our system, named LungTrack, hosted on commodity RFID devices for respiration monitoring. Our system retrieves subtle signal fluctuations at the receiver caused by chest displacement during respiration without need for attaching any devices to the target. It addresses the dead-zone issue and enables simultaneous monitoring of two human targets by employing one RFID reader and carefully positioned multiple RFID tags, using an optimization technique. Comprehensive experiments demonstrate that LungTrack can achieve a respiration monitoring accuracy of greater than 98% for a single target at all sensing locations (within $1^{st} - 5^{th}$ Fresnel zones) using just one RFID reader and five tags, when the target's orientation is known *a priori*. For the challenging scenario involve two human targets, LungTrack is able to achieve greater than 93% accuracy when the targets are separated by at least 10 *cm*.

CCS Concepts: • **Human-centered computing → Ubiquitous and mobile computing**.

Additional Key Words and Phrases: Respiration rate sensing, commodity RFID devices, dead zones, multiple targets

---

* This is the corresponding author

Authors' addresses: Lili Chen, Northwest University, International Joint Research Centre for Battery-free IoT, China, llchen@stumail.nwu.edu.cn; Jie Xiong, University of Massachusetts Amherst, USA, jxiong@cs.umass.edu; Xiaojiang Chen*, Northwest University, International Joint Research Centre for Battery-free IoT, China, xjchen@nwu.edu.cn; Sunghoon Ivan Lee, University of Massachusetts Amherst, USA, silee@cs.umass.edu; Daqing Zhang, Télécom SudPais, France, daqing.zhang@telecom-sudparis.eu; Tao Yan, Northwest University, International Joint Research Centre for Battery-free IoT, China, yantao@stumail.nwu.edu.cn; Dingyi Fang, Northwest University, International Joint Research Centre for Battery-free IoT, China, dyf@nwu.edu.cn.

Proc. ACM Interact. Mob. Wearable Ubiquitous Technol., Vol. 3, No. 3, Article 79. Publication date: September 2019.

79

1 INTRODUCTION

Respiration rate is one of vital signs that could provide insights into one's quality of sleep, general state of health, and underlying medical conditions. Typical respiration-related illnesses, such as apnea, affect more than 18 million Americans [10]. Continuous respiration monitoring plays an important role in both clinical and home settings. Clinically accepted tools to measure respiration rate, such as impedance pneumography [34] and capnography [15], are costly and intrusive, requiring frequent calibration and operation of instrument by trained professionals. More importantly, these methods do not lend itself for everyday use in home and community settings, as they often require invasive devices, such as nasal probes [1] and chest bands [2], for accurate respiration monitoring. Moreover, previous studies have reported that the elderly are reluctant to put on wearable devices in a daily basis and the infants may experience skin irritation with wearable devices [22, 45].

In the last few years, much research effort has been made to enable minimally-invasive or completely contactless approaches to alleviate the aforementioned issues with bulky wearable devices. For example, Hou *et al.* introduced an approach to attach lightweight, minimally obtrusive Radio Frequency Identification (RFID) tags on the target subject's clothes. However, this approach requires the user's efforts to carefully place the tags to clothes that the user wears in a daily basis, detach and re-attach the tags while washing the clothes, and is vulnerable to potential detachment of the tags from motion artifacts. Recent research has explored the possibility of employing RF signals for completely contactless respiration sensing. Adib *et al.* [13, 14] and Yue *et al.* [51] have leveraged Software-Defined Radio (SDR) with Frequency Modulated Continuous Wave (FMCW) radar signals, which are pioneer work in contactless respiration monitoring. However, these systems require dedicated device to support large bandwidth (several *GHz*) that is needed for achieving high accuracy. Recently, Wang *et al.* [48] and Zhang *et al.* [53] have successfully utilized commodity Wi-Fi devices for respiration monitoring by placing a transmitter and a receiver at separate locations, and analyzing the target-reflected signals received at receiver. However, one major issue associated with these studies is that the performance of respiration rate measurement cannot be made consistently throughout all the locations within the sensing range of the signal coverage. There exist a reasonable amount (> 50%) of such areas within the sensing range – referred to as *dead zones* – where the respiration sensing performance is poor even the target is close to the line-of-sight (LoS). Another well-known challenge for device-free sensing built on commodity device is to enable reliable system performance in the presence of multiple targets, where reflected RF signals from multiple targets are mixed together at the receiver and interfere with one another.

To overcome the above-mentioned issues associated with existing solutions, in this paper, we propose LungTrack, a contactless respiration rate sensing system based on commodity RFID devices. Taking an advantage of the fact that one RFID reader can communicate with multiple low-cost (i.e., a few cents) and small (i.e., sub-cm^2 range) tags that could be flexibly deployed in the environment, we analyze the amplitude and phase information of the RFID signals reflected from multiple tags and human targets – which could be easily accessible by commodity RFID readers – to monitor respiration rate in a contactless manner; note that the tags are not placed on the human body, but rather in the environment. More specifically, our system exploits the subtle RF signal changes caused by chest displacement during respiration. As illustrated in Fig. 1, when the human target inhales, the chest expands and consequently, the signal propagation path length decreases. On the other hand, when the target exhales, the chest contracts and the signal path length increases. This difference in the path length causes changes in both the amplitude and the phase of the resultant signal received at the RFID reader, which allows us to extract information regarding the respiration rate.

To turn our idea into a practice, we make the following efforts. First, we minimize the size of the "dead zones" associated with a single RFID tag by leveraging the unique complementary relationship between the amplitude and phase readings. More specifically, we report that 1) the "dead zones" when the amplitude readings are solely used for sensing and 2) the "dead zones" for the phase readings do not overlap and are complementary to each other. Thus, we combine the amplitude and the phase readings of the resultant signals to substantially reduce the size of the dead zones associated with a single RFID tag. Then, we incorporate multiple RFID tags to further reduce the size of the overall "dead zones" within the sensing area. The premise of these methods is to know the orientation and location range of the target. Second, we explore the possibility of exploiting commodity bandwidth-limited RFID device to support contactless respiration monitoring when multiple human targets present in the sensing area (e.g., two individuals sleeping on the same bed). Because the respiration rates do not vary dynamically among human subjects, conventional frequency-domain signal decomposition methods do not work effectively to identify the respiration information associated with each target. In this paper, we propose to take an advantage of the existence of "dead zones" of RFID tags to address the above-mentioned issue. We introduce a method to carefully allocate the
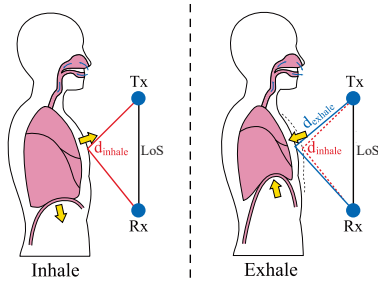
Fig. 1. A conceptual illustration of how RF signal paths change from body movements during respiration. When the target inhales, the chest expands and consequently, the signal propagation path length is decreased. In contrast, when the target exhales, the chest contracts, which increases the path length.
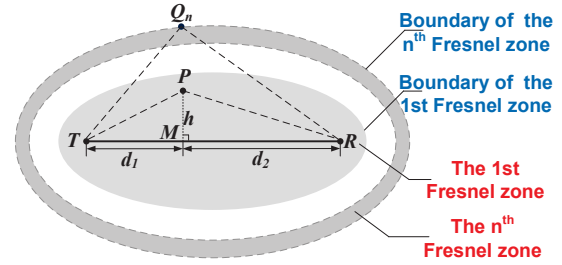

Fig. 2. An illustration of the Fresnel zones. T and R represent the signal transmitter and receiver, respectively. P represents a human target when it is located in the first Fresnel zone, and Q_n represents a human target in the nth Fresnel zone.

RFID reader and tags in the environment, such that each tag's "dead zone" is positioned to overlap with different human targets (i.e., eliminating the interference). For example, in a scenario where a single reader and two tags are used to monitor respiration of two human targets lying on the same bed, the first tag can be positioned such that its "dead zones" include the location range of the second human target, so that the reflected signals of the first tag only captures information about the first target's respiration. Similarly, the second tag can be positioned such that its "dead zone" overlaps with the location range of the first target. Although the proposed method is limited to scenarios in which each target's chest location cannot dynamically change beyond a range of $60 \times 70\ cm^2$, and the two targets need to be separated by at least 10 cm, it can still be applied to a variety of applications in respiration rate monitoring (e.g., on-bed or in-car). We also discuss the theoretical framework to identify the optimal locations of the sensing components (i.e., RFID tags) using an optimization technique. Last, we implement a prototype of LungTrack using commodity RFID devices and validate its performance for monitoring respiration rate through a series of experiments including both sitting and lying scenarios. Our results show that LungTrack can achieve above 98% accuracy at all locations within $1^{st} - 5^{th}$ Fresnel zones with just one RFID reader and five tags. We also compare LungTrack with the most relevant Wi-Fi signal-based respiration rate monitoring approach, namely FullBreathe [52]. We show that LungTrack, with only one tag utilized, yields substantially smaller "dead zones" (i.e., 20% of the approximately $1.5 \times 2\ m^2$ sensing range) when compared to FullBreathe (i.e., 35%). Furthermore, we examine LungTrack's robustness towards multiple targets, as well as the target's posture (sitting vs. lying), sitting orientation, sleep orientation, chest thickness, and age.

The key technical contributions of this work include the followings:

- To the best of our knowledge, this work is the first attempt to achieve a contactless respiration sensing and minimize "dead zones" using commodity RFID device.
- We utilize the complimentary property of the resultant RF signal's amplitude and phase information to minimize the size of the "dead zone" associated with a single RFID tag. Then, we deploy multiple tags to further minimize the remaining "dead zones." We show theoretical analysis and experimental validation of the proposed method.
- We design, implement and evaluate LungTrack's performance. Experimental results show that our system can achieve high respiration sensing accuracy with just one commodity RFID reader and five low-cost tags.

2 PRELIMINARIES

In this section, we discuss the fundamentals of the Fresnel diffraction and reflection models in free space, which supports the theoretical foundation of LungTrack to enable contactless respiration monitoring via RFID signals.

2.1 Fresnel Diffraction and Reflection Models

In the context of RF signal propagation in free space, Fresnel zones are concentric ellipses with the transmitter T and receiver R at two focal points, which are used to represent regions (i.e., zones) of different RF signal propagation strength between T

and R (see Fig. 2). The innermost ellipse is the First Fresnel Zone (FFZ), representing the area where the direct LoS signals can pass through. The nth Fresnel zone corresponds to the area between the $(n-1)^{\text{th}}$ and n^{th} ellipses. The outer boundary of the nth Fresnel Zone is composed of reflection points Q_n as shown in Fig. 2 that satisfy:

$$|T, Q_n| + |Q_n, R| - |T, R| = \frac{n\lambda}{2}, \tag{1}$$

where λ is the wavelength of the signal, and $|X, Y|$ represents the Euclidean distance between two points X and Y. Furthermore, we denote the distance from any of one target points P to the line-of-sight (LoS) as h (i.e., $h = |P, M|$), as shown in Fig. 2. Using the new point M, the path TR can be divided into two segments: $d_1 = |T, M|$, and $d_2 = |M, R|$. The path difference Δd between the path TPR and the LoS path TR is calculated by:

$$\begin{aligned} \Delta d &= |T, P| + |P, R| - |T, R| \\ &= d_1\sqrt{1 + (h/d_1)^2} + d_2\sqrt{1 + (h/d_2)^2} - (d_1 + d_2). \end{aligned} \tag{2}$$

This path difference can be used to derive the phase difference between the target signal path and the direct LoS path as the following:

$$\Delta\varphi = \frac{2\pi\Delta d}{\lambda}. \tag{3}$$

When the human target is located outside of the FFZ, the reflection dominates [35, 48, 53]. On the other hand, when the target is inside the FFZ, diffraction dominates. Based on this phenomenon, We discuss the effects of diffraction and reflection below.

Diffraction effect: When the target P is located inside the FFZ, we have $h \ll d_1$ and $h \ll d_2$. Thus $(h/d_1)^2 \ll 1$ and $(h/d_2)^2 \ll 1$. According to the approximation equation $\sqrt{1+x} \approx 1 + \frac{x}{2}$ when $x \ll 1$, Equation (2) can be simplified as:

$$\Delta d \approx \frac{h^2}{2}\frac{d_1 + d_2}{d_1 d_2}. \tag{4}$$

The received signal due to diffraction can now be computed as

$$S_{dif} = A(v) \cdot e^{-2j\varphi_{dif}}, \tag{5}$$

where φ_{dif} represents the phase of diffraction signal and $v = h\sqrt{\frac{2(d_1+d_2)}{\lambda d_1 d_2}}$ represents the Fresnel-Kirchhoff diffraction parameter [35]. $A(v)$ is the amplitude of the diffraction signal, which is a function of v and could be computed using the following equation [35]:

$$A(v) = \frac{1+j}{2} \cdot \int_v^\infty e^{\frac{-j\pi x^2}{2}} dx, \tag{6}$$

where j is an imaginary number.

Reflection effect: When the target P is located outside the FFZ, reflection dominates. Different from Wi-Fi, which has only one reflection path ($T \to P \to R$), there exist multiple reflection paths for an RFID system due to the round-trip propagation. For an RFID system employing a single tag, there exists three paths:

  (i) *Reader* $\to$ *Tag* $\to$ *P* $\to$ *Reader*
  (ii) *Reader* $\to$ *P* $\to$ *Tag* $\to$ *Reader*
  (iii) *Reader* $\to$ *P* $\to$ *Tag* $\to$ *P* $\to$ *Reader*

The reflection signal at the reader is a superposition of these three paths:

$$S_{ref} = \Sigma_{i=1}^3 (A_{ri} \cdot e^{-j\varphi_{ri}}), \tag{7}$$

where A_{ri} represents the attenuation and initial phase of the ith reflection path, φ_{ri} is the phase change due to the propagation of the ith reflection path.
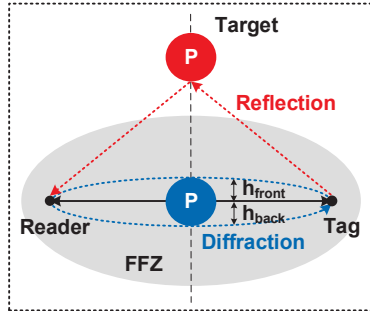
Fig. 3. Diffraction and reflection effects of the RF signal when the target is located within and outside the FFZ, respectively. The diffraction signal have two paths passing through two sides of the target (e.g., front and back).
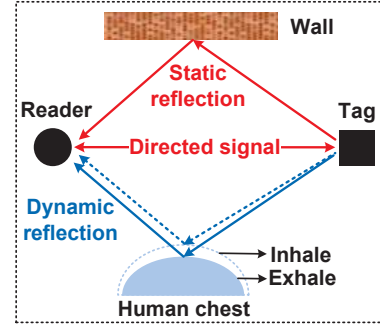

Fig. 4. The received signal is a superposition of multiple signals including the direct path, the reflected signals from the human target, and the reflected signals from static objects in the environment.

2.2 The Effect on the Received RF Signal When a Target is Present

When a target is present, based on the location of the target, we can obtain the resultant received signal as below with the model presented in Section 2.1 [53]:

$$S = \begin{cases} A_d \cdot e^{-j2\varphi_d} + S_{dif}, & \text{Within the FFZ} \\ A_d \cdot e^{-j2\varphi_d} + S_{ref}, & \text{Outside the FFZ} \end{cases}, \tag{8}$$

where A_d and φ_d represent the attenuation and initial phase of the LoS signal, respectively. In practice, when a target P is within the FFZ, the diffraction signal S_{dif} needs to be more carefully modeled. Because the target has a non-negligible size and cannot be simplified as a single point, we have to consider two diffraction signals that pass through two different sides of the target (e.g., front and back of the body), as illustrated in Fig. 3. Considering this practical phenomenon, the total diffraction signal can be expressed as [53]:

$$S_{dif} = A(v_{front}) \cdot e^{-2j\varphi_{dif,front}} + A(v_{back}) \cdot e^{-2j\varphi_{dif,back}}, \tag{9}$$

where v_{front} and v_{back} are the front diffraction parameter and back diffraction parameter, respectively. On the other hand, when the target is outside of the FFZ, the reflection signal is reflected from only one side of the target, as illustrated in Fig. 3. Consequently, the equation for the reflection signal remains identical as (7). In this work, to better indicate the target's relative position in the Fresnel zones, we define a coefficient, namely the Fresnel-zone coefficient: $k = \frac{|Tag,P|+|P,Reader|-|Tag,Reader|}{\lambda/2}$. The value of $k \leq 1$ indicates that the target is within the FFZ, and the value of $N - 1 < k \leq N$, where N represents the number of Fresnel zones and $N \geq 2$, indicates that the target is within the Nth Fresnel zone. For a human target with a non-negligible size in the FFZ, we utilize two of these coefficients k_{front} and k_{back} to precisely represent the target's front chest and back positions.

3 MODELING HUMAN RESPIRATION

Guided by the theories presented in Section 2, we model the process of human respiration when the target is located at different RFID Fresnel zones. We also analyze the effects of the chest orientation on respiration sensing.

3.1 Modeling the Respiration Process with Signal Variations

When a human target breathes, the chest displacement causes the path length of the target-related signal to change as shown in Fig. 4. The chest displacement during respiration is around $0.5\ cm$ [32]. Although small, this subtle displacement induces a significant amount of phase changes at the reflected signal. For example, when the target is inside the FFZ, a $0.5\ cm$ chest displacement causes a signal path change of approximately $1\ cm$. For the RFID system with a round trip propagation, the
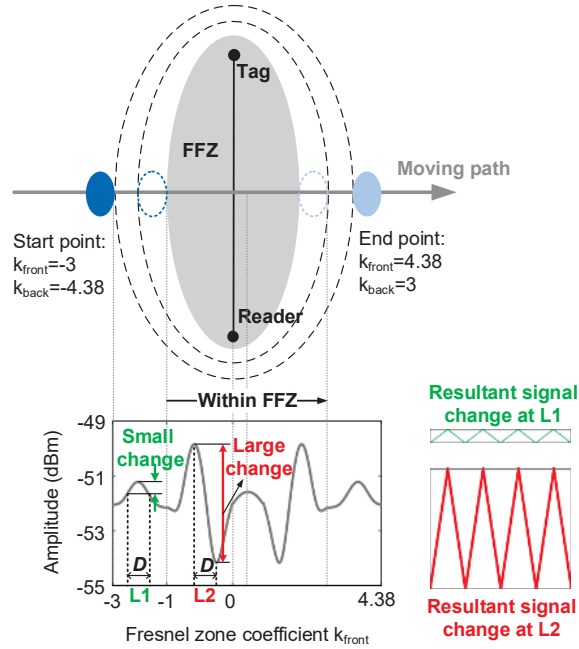
Fig. 5. Amplitude changes of resultant signal with chest movement. The figure shows a same amount of chest displacement occurs at different locations (L1 and L2), causing very different amplitude variations of the received signal. Note that the range of "within FFZ" is from $k_{front} = -1$ to $k_{back} = 1$, considering the target thickness.

associated phase change can be easily computed (i.e., $22.5°$ in this example). However, in practice, besides the respiration-induced reflection path, there is a direct path, as well as reflection paths from other objects in the environment. Hence, the received signal at the receiver is a superposition of multiple signals, as conceptually illustrated in Fig. 4. When multiple signals are mixed, the phase change of the received signal cannot be easily derived, and we need to use Equation (8) to obtain the resultant signal based on where the target is located (i.e., inside or outside the FFZ). For simplicity, let us assume that the target is facing the LoS of the transceiver pair and located on the perpendicular bisector at the boundary of the third Fresnel zone. Let us further assume that the length of the LoS path is 1.5 m and the target has a chest thickness of 16 cm. Fig. 5 shows the behavior of the signal amplitude (i.e., resultant of (8)) when the location of the human target changes (i.e., the target walks to the other side of boundary of the third Fresnel zone), bisecting the LoS between the reader and the tag. Fig. 5 verifies that the behavior of the signal amplitude can vary significantly at the two locations even the chest movement D is kept fairly constant. When the chest displacement occurs at where the signal amplitude changes substantially (e.g., L2), respiration could be easily detected. On the other hand, it is difficult to detect respiration when the amplitude changes are relatively small (i.e., L1), which is referred as a "dead zone" in this work. Moreover, when the target is located far away from the LoS path, the signal changes caused by respiration are much weaker. To achieve robust sensing performance, the target is thus confined within the first five Fresnel zones (from 1st to 5th) of the tag-reader pair in our system.

3.2 Verifying the Fresnel Models with RFID

To verify the Fresnel diffraction and reflection models, we conducted a benchmark experiment using a dummy chest with dimensions as shown in Fig. 6 (a). Fig. 6 (a) also shows the experimental setup, where the passive tag and reader were placed at the same height (1 m) with a distance of 1.5 m between them. We moved the dummy chest slowly across the Fresnel zones with k_{front} changing from -5 to 6.55. Fig. 6 (b) and (c) compares the results obtained from the experiment to the theoretical

(a) Experimental settings.

(b) The one reflection path model.
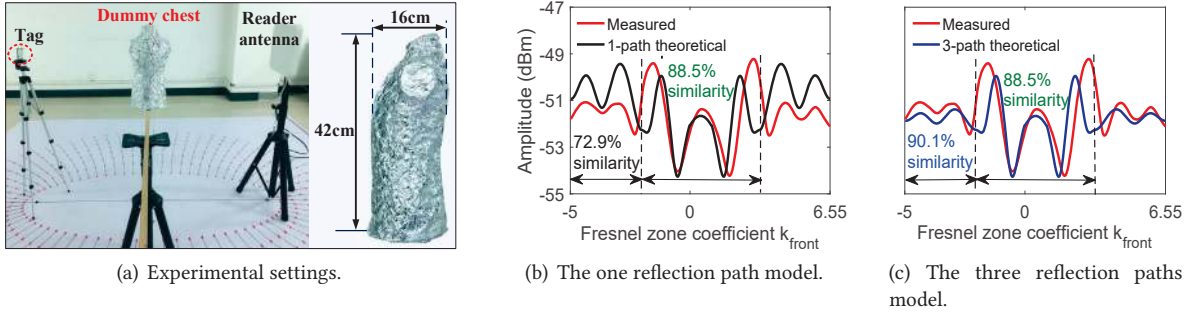
(c) The three reflection paths model.

Fig. 6. Comparison of experimental result and theoretical results. The percentages in the figure represent the similarity between the two curves calculated with the modified dynamic time warping (DTW) method [11].

model. We can see that in the $2^{nd} - 5^{th}$ Fresnel zones where reflection dominates, the proposed three-path model in Fig. 6 (c) (i.e., (7)) is more accurate than the one-path model in Fig. 6 (b). Note that the theoretical plots are not smooth at the boundary of the FFZ because we employ the diffraction model within the FFZ and the reflection model outside the FFZ. In practice, there still exists a small amount of reflection within the FFZ and diffraction outside the FFZ near the boundary, which contributes to the discrepancies between the theoretical model and the experimental results.

3.3 Impact of the Target Orientation

In practice, even at the same location, the target may face different orientations. To investigate the effects of the target orientation to the respiration sensing performance, we rotated the dummy target $360°$ at a step size of $1°$, starting from the orientation that bisects the LoS path perpendicularly (i.e., $0°$), as shown in Fig. 7. The target's chest displacement D_{front} and back displacement D_{back} due to respiration were set to $0.5\ cm$ and $0.2\ cm$, respectively. The heatmap in Fig. 7 shows that when the target is facing the LoS (i.e., $0°$), we achieve the best sensing performance because the front chest makes the largest movements during respiration [32]. The worst orientation for sensing was when the target's face direction was parallel to the LoS (i.e., $90°$ and $270°$) because the side-to-side shoulder movements during respiration is minimal and thus, difficult to be captured. We also notice that when the target's back is facing the LoS (i.e., $180°$), the sensing performance was still acceptable from a reasonable backside movement.

4 HUMAN RESPIRATION RATE SENSING

In this section, we first describe the fundamentals underlying the respiration rate detection from the received RFID signals. Then, we introduce our contributions to minimize the amount of "dead zones" and multi-target signal interference in order to achieve robust respiration rate sensing.

4.1 Respiration Rate Extraction from Received Signal

The fundamentals of respiration detection are established on the fact that movements of the human body during the periodic inhaling and exhaling process introduce cyclical peaks and valleys to the received RF signals. However, there exist a number of challenges to enable reliable respiration rate detection: (i) there may exist interference from nearby individuals other than the target; (ii) the target may introduce motion artifacts from in-place activities of daily living (e.g., typing, calling, walking, or even running). Such events may introduce multipath effects and thus, undesired noises to the received signal, as shown in Fig. 8 (top). To deal with such dynamic interference, we first reduced the noise components of the received signal using the method introduced in [44] to smooth the time-series of phase and amplitude information based on a moving average filter. Then, a band-pass filter (i.e., Butterworth filter with cut-off frequencies between $0.05\ Hz$ and $0.8\ Hz$) was applied to attenuate high-frequency components of the signal that correspond to the non-respiration-related activities (e.g., multipath effects or motion artifacts). For example, the respiration frequency ranges from $0.1\ Hz$ to $0.7\ Hz$ whereas that of typical human
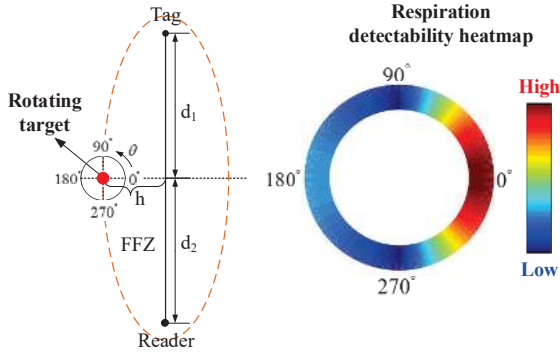
Fig. 7. Impact of target orientation θ (k_{front} = 1). Left: setup. Right: the visualization of respiration detectability. The red color indicates good detection performance, while the blue color indicates the performance is poor.
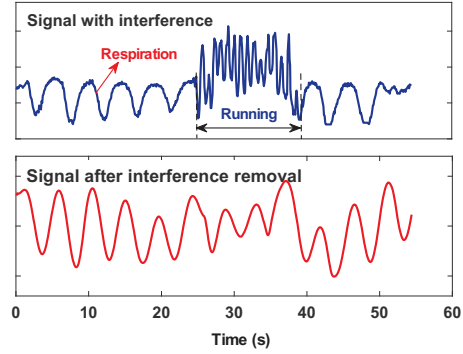

Fig. 8. Extracting respiration from interfering movement. The figure shows that by conducting frequency domain filtering to the signal suffered activity interference (running), we are still able to obtain clear fluctuation cycles of respiration.

movements is much higher. Finally, we detected local peaks on the time-domain, band-pass filtered signals using the method presented in [30]. The respiration rate is calculated as the number of peaks divided by the time interval. Fig. 8 illustrates an example of applying filter for obtaining clear respiration cycles, when the signal was significantly disrupted by a vigorous human activity (e.g., running on a treadmill).

4.2 "Dead Zone" Removal

It is demonstrated in Section 3.1 (see Fig. 5) that respiration sensing performance is dependent on the target's position with respect to the locations of the reader and the tag. Such "dead zones" could significantly degrade the sensing performance when the system is deployed in practice. For example, approximately 3–5 *cm* changes in the body position on a bed during sleep can place the target at a tag's "dead zone" where the respiration can hardly be monitored. To enable stable, long-term respiration monitoring in real-world settings, the issues of "dead zones" must be addressed so that respiration sensing can be made accurately and reliably within the entire sensing area (e.g., entire bed).

Before discussing our technique to minimize the amount of "dead zone", we first visualize "dead zones" when only amplitude or only phase reading is used for the respiration sensing, and discuss their unique complementary relationship – the fundamental characteristic that we leverage to substantially reduce the amount of "dead zones" in the sensing area. With an assumption that the orientation of the target is fixed to face the LoS, for simplicity, the respiration sensing capability enabled by only the amplitude readings is visualized in Fig. 11. The warmer (red) colors indicate large amplitude changes caused by respiration movement thus good sensing performance within the sensing area, whereas the cooler (blue) colors indicate poor sensing performance. Considering the signal amplitude changes below an empirical threshold (i.e., 0.3 *dBm*) as the "dead zones", 76% of the sensing area was determined to be "dead zones". In a similar manner, when only the phase readings were used for the respiration sensing, 71% of the locations were identified as "dead zones" (where the phase changes below an empirical threshold of 0.033 *rad*), as shown in Fig. 12. Interestingly, we can observe that the dead zones of amplitude and phase readings do not overlap and are complementary to each other in terms of sensing capability. In other words, this implies that when the amplitude has a small variation and cannot achieve accurate respiration monitoring, phase reading has a larger variation to enable relatively accurate monitoring (see the following paragraph for details). Inspired by these findings, contrary to past work that employed either the signal amplitude [48] or signal phase [14] information for respiration sensing, we propose a fusion technique that **combines the amplitude and phase information** to reduce the amount of "dead zones".

The theory behind this unique complementary relationship (in terms of "dead zones") between the amplitude and phase information can be explained based on the fact that the respiration sensing capability is dependent on the amount of signal
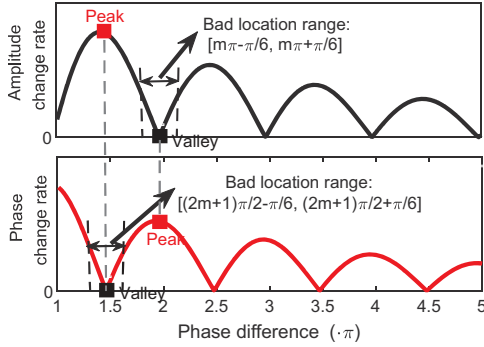
Fig. 9. Complementary principle between amplitude and phase information for respiration sensing (in $2^{nd} - 5^{th}$ Fresnel zones, $m = 1, 2, \ldots, 5$). The greater rate of signal amplitude/phase change indicates the better respiration sensing capability.

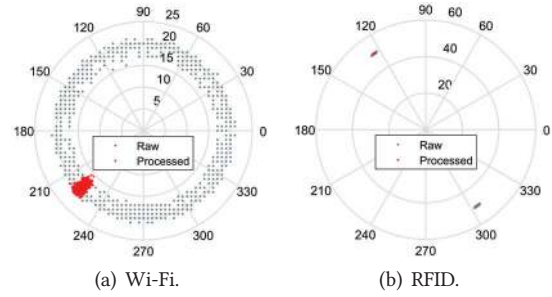

(a) Wi-Fi.   (b) RFID.

Fig. 10. Phase information comparison between Wi-Fi and RFID. It can be seen that the raw phase information obtained by commodity WiFi NIC behaves extremely random over the all feasible field. Even utilizing the phase shift removing method [52], the processed phase in Wi-Fi is still less stable than that in RFID.

variation induced by the body (chest) movements of the target. Since the chest displacement caused by respiration is very small, the amount of signal variation is linearly related to the change rate (i.e., derivative) of the signal amplitude/phase curve generated as the chest moves along a straight line. Fig. 9 shows the change rate of both the signal amplitude and phase. A larger value of change rate represents higher respiration sensing capability. It is obvious from the figure that when the amplitude slope is at a valley, the phase slope actually reaches a peak, which means that respiration sensing capabilities by utilizing the signal amplitude and phase are complimentary to each other. The complementarity is also proved in Wi-Fi [52]. However, combining amplitude and phase in Wi-Fi induces limited improvement in reducing the "dead zones" for respiration sensing, because the raw phase information collected from commodity Wi-Fi device that employs off-the-shelf Network Interface Cards (NIC), such as Intel 5300 [19], is very coarse (see Fig. 10) due to random noise and unsynchronized time clock between the transmitter and receiver [29, 52]. Even utilizing the phase shift removing method [52], the processed phase in Wi-Fi is still not as stable as in RFID. Also, the amplitude information in Wi-Fi is noisier than that in RFID.

An obvious question that follows is how do we take advantage of both phase and amplitude for respiration sensing? To answer this, we compare the variation range of phase and amplitude, and choose the information with a larger variation range and thus the clearer periodic cycles. Note that there exists a multiplicative factor (set to be nine since the maximum amplitude variation is approximately nine times the maximum phase variation), since their variation range are not in the same order of magnitude. The new heatmap after combining amplitude and phase is presented in Fig. 13. We can see besides the perfect complementarity in $2^{nd} - 5^{th}$ Fresnel zones, there is also a certain degree of complementarity in the FFZ. The total amount of "dead zones" is reduced from 71% to 60%.

Even after combining phase and amplitude readings as shown in Fig. 13, there exist still a large amount of remaining "dead zones". To further reduce the amount of "dead zones" in the monitoring area, we fully take advantage of tag's low price and scalability (which is otherwise not possible with Wi-Fi devices). Our approach is to deploy multiple tags at different locations within the sensing area such that their "dead zones" are complemented by each other. As shown in Fig. 14, by randomly adding one more tag, the amount of "dead zones" was reduced from 60% to around 40%. Note that one reader can communicate with multiple tags simultaneously, hence the hardware cost of employing multiple tags remains approximately the same.

The key challenge here is to optimize the distribution (i.e., positions) of multiple tags to minimize the amount of the overall "dead zones" in the sensing area. Suppose we deploy a total number of N tags and T_p is the pth ($p = 1, 2, ..., N$) tag. The pth tag's position is defined as L_p. We want to obtain the deployment locations for the N tags $[L_1, L_2, \cdots, L_N]$ so the amount of "dead zones" is minimized. The percentage of "dead zone" J is expressed as:

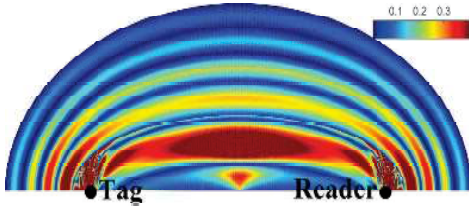$$J = 1 - \frac{\bigcup_{p=1}^{N} F(L_p)}{Z},$$ (10)

Fig. 11. Visualization of the good locations associated with a single RFID tag when using only amplitude readings (23.58%).
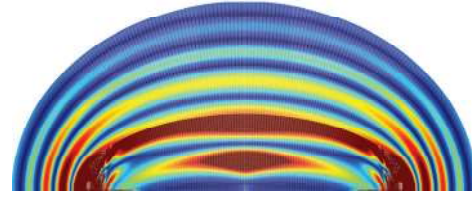

Fig. 12. Visualization of the good locations associated with a single RFID tag when using only phase readings (28.84%).
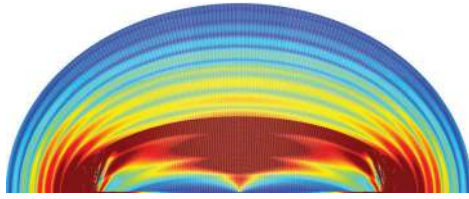

Fig. 13. Visualization of the good locations associated with a single RFID tag when combining amplitude and phase readings (39.75%).
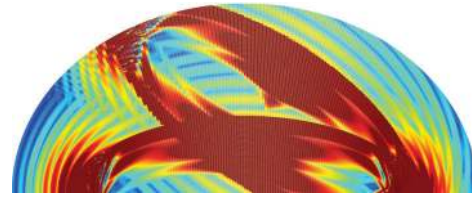

Fig. 14. Visualization of the good locations as randomly adding one more tag after combining amplitude and phase readings (59.65%).

where Z is the total number of grids in monitoring area and $F(L_p)$ is the number of grids at which good sensing performance can be achieved with the pth tag. J is a non-linear function due to the Fresnel diffraction integration. We thus used the multi-objective genetic algorithm to compute the optimal tag placement. The L_p can be specified as (ang_p, dis_p), where ang_p is the angle between p^{th} tag's direction with respect to the reader and the maximum radiation direction of reader, and dis_p is the distance between the pth tag and the reader. Considering the directionality of the antenna of the reader and the communication distance between the reader and the tag, we empirically added the constraints of $-\pi/3 \leq ang_p \leq \pi/3$ and $0.5\ m \leq dis_p \leq 2.5\ m$ to the optimization problem. Fig. 15 shows that by carefully deploying five tags, our system can achieve good sensing performance at 99% of the locations in the $1^{\text{st}} - 5^{\text{th}}$ Fresnel zones.

Effect of the frequency diversity in RFID. RFID systems hop channels due to security reasons. We would like to see if frequency hopping helps remove the "dead zones." The basic intuition is that while a location is "bad" for one frequency channel, it may be "good" for another channel. Suppose the target is located at the mth Fresnel zone boundary, which is a bad location for channel f_1. The path difference Δd between the reflection path and the LoS path can be represented as $\frac{mc}{2f_1}$, where c is the speed of light. This path difference results in a phase difference of $m\pi$. Note that the bad location range of using amplitude information for respiration sensing is between $m\pi - \pi/6$ and $m\pi + \pi/6$, as shown in Fig.9. Thus, we need another phase change of $\pi/6$ to turn the bad location into a good location. When the reader hops to another frequency channel f_2, the phase change caused by frequency hopping is $\Delta\Psi = 2\pi(\frac{\Delta d}{c/f_1} - \frac{\Delta d}{c/f_2})$. Therefore, the phase change $\Delta\Psi$ needs to satisfy $\Delta\Psi \geq \pi/6$ to turn the bad location into a good location. By placing $\Delta\Psi$ into this constraint equation, we obtain the following result:

$$\frac{f_1}{f_2 - f_1} \leq 6m. \tag{11}$$

In other words, for frequency hopping to work in the second Fresnel zone ($m = 2$), the frequency difference $f_2 - f_1$ needs to be larger than 80 MHz. However, the frequency range of the RFID system is only 26 MHz. So frequency hopping may be an effective method for Wi-Fi with a much larger frequency range, it does not work well with RFID systems.
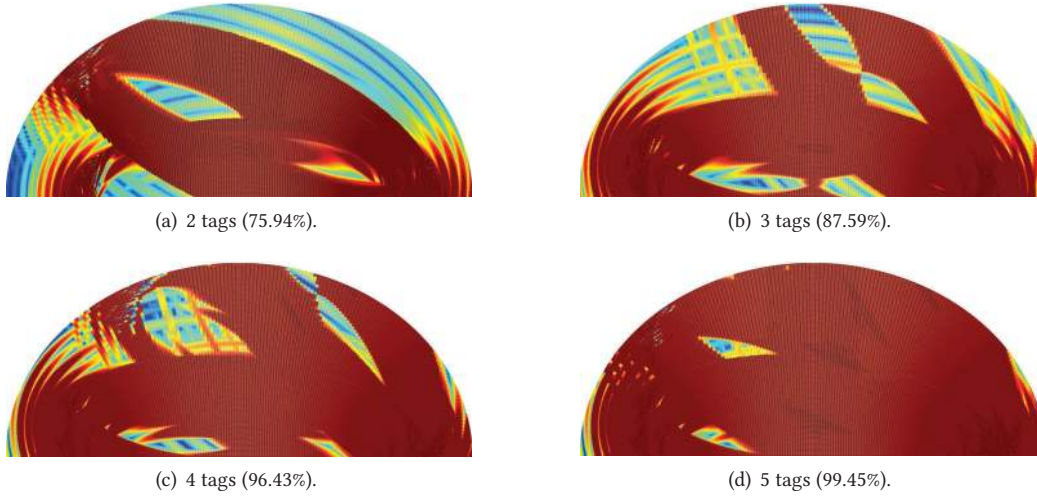
(a) 2 tags (75.94%).

(b) 3 tags (87.59%).

(c) 4 tags (96.43%).

(d) 5 tags (99.45%).

Fig. 15. Visualization of good locations as carefully placing multiple tags (theoretical results).

4.3 Multi-person Monitoring

This section discusses the challenging issue of multi-person respiration sensing. For example, how can we monitor the respiration of each individual accurately when a couple sleeps on the bed during the night? Since the two targets are generally separated less than 1 m away in such a scenario, the reflected signals from both targets are mixed together, which makes it difficult to sense the respiration for either of them [14]. Traditional methods rely on converting the signal to frequency domain but this only works when the two targets' respiration rates are dramatically different, which is unlikely in real-world settings. The latest research [51] formulated the problem as blind source separation and utilized Independent Component Analysis (ICA) to separate multiple targets' respiration. This method achieved high resolution on the premise of wide frequency bandwidth but this, unfortunately, is unavailable in RFID. In this paper, we aim to distinguish the respiration rates of multiple targets from a new angle. The crux of the proposed method is to **utilize the "dead zones"** of multiple RFID tags for eliminating the signal interference reflected from multiple targets. Unlike the single target respiration monitoring scenario where we leveraged multiple tags to remove the "dead zones," in multi-target scenario, we take an advantage of the "dead zones" by carefully positioning each tag such that the associated "dead zones" could be used to detect respiration of only a single target.

We take the sleeping scenario as an example to illustrate our method but our method can be generalized to other multi-target sensing problems. As shown in Fig. 16, Z_1 and Z_2 represent the sensing areas for Person 1 and Person 2, and T_1 and T_2 represent the two tags used for respiration monitoring. As described in previous sections, there exist "dead zones" of each tag where respiration can not be sensed. Assuming that the target's chest stays within the sensing area (i.e., Z_1 and Z_2), we utilize the "dead zones" to mitigate the interference from the other person. For example, we can carefully position T_1 such that Person 1's chest is located at the sensible zones of T_1 while Person 2's chest is within the "dead zones" of T_1. This will allow T_1 to capture the respiration of Person 1 only. Similarly, T_2 can be positioned to monitor Person 2's respiration only. Assuming a fixed monitoring area defined for each target, finding the optimal locations of the reader and the tags becomes an optimization problem. We optimize the locations of the reader, T_1, and T_2 by maximizing a cost function O:

$$O = P_{1,1} + N_{2,1} + P_{2,2} + N_{1,2}, \tag{12}$$

where $P_{1,1}$, $N_{2,1}$, $P_{2,2}$ and $N_{1,2}$ represent the number of sensible zones[1] in Z_1 for T_1, the number of dead zones in Z_2 for T_1, the number of sensible zones in Z_2 for T_2 and the number of dead zones in Z_1 for T_2, respectively. Fig. 17 shows the

---

[1]We divide the monitoring region into small grids and choose the center point of the grid to evaluate if it is a sensible zone or a dead zone.
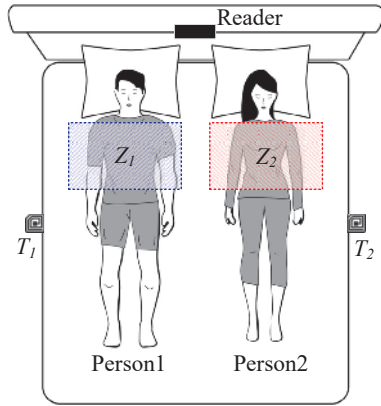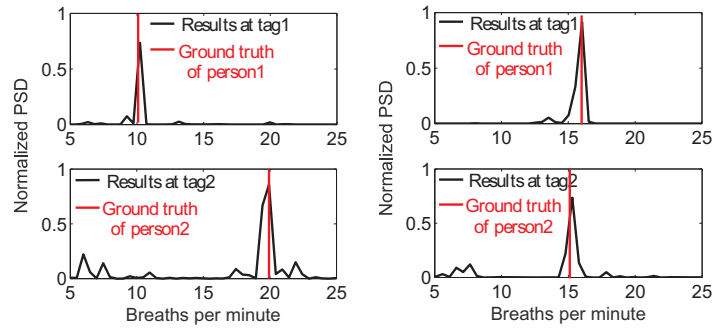
Fig. 16. Couple respiration monitoring during sleep.

(a) Very different respiration rates: 10 (Person1) and 20 (Person2).

(b) Similar respiration rates: 16 (Person1) and 15 (Person2).

Fig. 17. Estimated results of different respiration patterns. The ground truth is obtain by asking the target to wear a finger pulse oximeter [6].

(a) Single-target siting scenario.

(b) Single-target lying scenario.

(c) multi-target scenario.

Fig. 18. Real experimental deployment.

two-person respiration sensing performance with our method. We can see that regardless of the difference in the respiration rates between two targets, our method is capable of accurately monitoring each target's respiration rate.

In practice, the user needs to input the sensing area and the number of tags they want to deploy. Then, our system can output the optimal locations for reader and tags. Since the physical size of the reader is not as small as the tags, the user can also first determine the location of the reader according to their preferences and take the reader's location as a constant in the optimization process. Based on the empirical distribution of sensible zones of a single tag (after combining the amplitude and phase information as discussed in Section 4.2), each person's chest can move within a sensing area of $60 \times 70\ cm^2$, which is sufficiently large for practical sleep monitoring deployment.

5 EVALUATION

We implemented our system using commodity RFID devices. Comprehensive experiments are conducted to validate the proposed model and evaluate the system performance.

5.1 Implementation

The hardware of LungTrack is composed of three commodity components: a commercial off-the-shelf (COTS) ImpinJ Speedway R420 RFID reader [7], a directional RFMAXS9028PCRJ antenna [8] for the reader, and UHF Alien H47 tags [4]. The reader is adopted without any hardware or firmware modification. It is compatible with the EPC Gen2 standard [5] and operates in the UHF band ranging from 920.675 MHz to 924.375 MHz. We utilize the timestamp function provided by the reader for the data
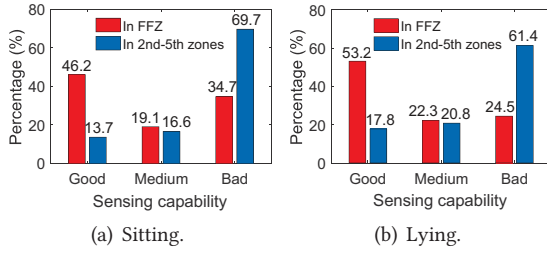
Fig. 19. Respiration detectability at two postures. The better sensing capability for lying posture is because when target lies, the respiration causes movement at both front chest and back while when target sits, the respiration causes larger front chest displacement.
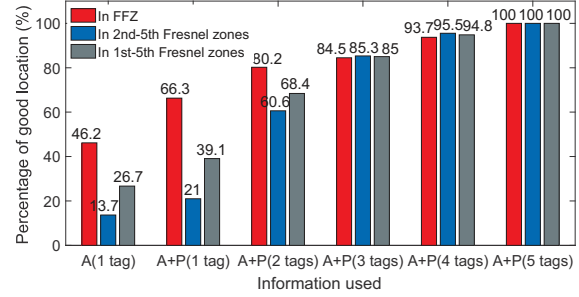

Fig. 20. Effectiveness of "dead-zone" removing schemes we proposed. It can been seen that with 5 tags deployed, LungTrack can remove all "dead zones" within the test area.

samples. The experiments were carried out in an open room with a size of $6m \times 8\ m^2$, and a home environment with a sofa, a television, a furniture, and a queen-size bed, as shown in Fig. 18 (c). In the single target scenario, we consider two typical postures, i.e., sitting and lying, as shown in Fig. 18 (a-b). For the sitting posture, we set the reader and tag height as $1\ m$ above the ground. For the lying posture, the default height of reader and tag is $0.8\ m$. The default reader and tag distance was set as $1.5\ m$. The default orientation of the target was to face the middle point of the LoS.

In this work, we define the detection accuracy as following:

$$Accuracy = \frac{1}{C} \sum_{c=1}^{C} (1 - \frac{|R_{m,c} - R_{t,c}|}{R_{t,c}}),$$

(13)

where C is the number of experimental trials, and $R_{m,c}$ and $R_{t,c}$ represent the measured and ground truth of the respiration rate in the cth trial, respectively. The absolute difference between the measured and ground truth of the respiration rate $|R_{m,c} - R_{t,c}|$ represents the monitoring error. We asked the target to wear a finger pulse oximeter [6] to obtain the ground truth respiration rate in controlled experiments focusing on the validation of the proposed algorithms. For experiments that monitoring respiration rates for a long-term period in near-realistic settings – because the pulse oximeter was not able to record data for long-term – we video-recorded the chest movements of subjects and manually annotated the respiration rates.

5.2 System Performance

5.2.1 Overall Accuracy with One RFID Tag. In this experiment, we recruited ten student participants ($20 - 28$ years old) to evaluate the performance of LungTrack. The participants wore their daily clothes of various materials. The participants had varying heights, weights and chest thicknesses. Based on the respiration sensing accuracy, we grouped the sensing zones into three categories: **Good**: $Accuracy \geq 98\%$; **Medium**: $85\% \leq Accuracy < 98\%$; and **Bad**: $Accuracy < 85\%$. Any sensing zones with $Accuracy$ greater than or equal to 85% was considered as **detectable**. We divided the $1^{\text{st}} - 5^{\text{th}}$ Fresnel zones on one side of the LoS into 100 grids and evaluated the respiration sensing performance when the target was located at the center of each grid. The target breathed naturally during the experiment. The overall performance is shown in Fig. 19. For sitting scenario, our system could achieve above 98% of accuracy for respiration rate detection at 46% of the areas in the FFZ and and 14% of the areas in the $2^{\text{nd}} - 5^{\text{th}}$ Fresnel zones, when averaging the results of ten targets. These experimental results are quite close to the theoretical results that we discussed in Section 4.2. When subjects were lying on a bed, the detection accuracy increased to 53% and 18% for the first and the remaining Fresnel zones, respectively. It is noteworthy that the reader and tag are adjusted to different heights depending on the target location within the $1^{\text{st}} - 5^{\text{th}}$ Fresnel zones. We believe we could obtain a greater detection accuracy when the subjects were lying on a bed because the font chest movements were much larger than the sitting posture. This larger displacement of the chest movements leads to greater signal variations and accordingly, better respiration sensing performance.
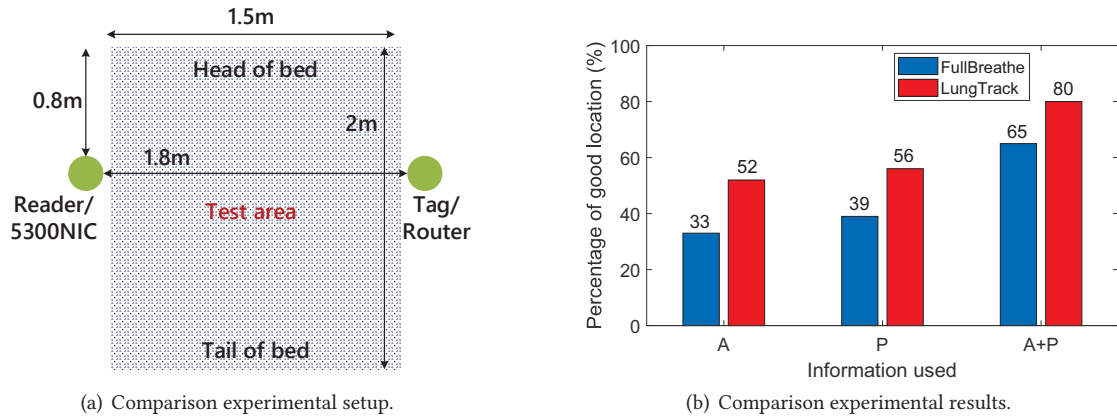
(a) Comparison experimental setup.

(b) Comparison experimental results.

Fig. 21. Effectiveness comparison of complementarity based "dead zone" removal schemes between Wi-Fi based approach (Full-Breath) and LungTrack.

5.2.2 Effectiveness of Removing "Dead Zones". Here we verify the effectiveness of two proposed methods for removing the "dead zones."

Employing the complementarity between amplitude (A) and phase readings (P): We show the results by combining phase and amplitude in Fig. 20. The percentage of good locations increases significantly from 46% to 66% in FFZ, and from 14% to 21% in the $2^{nd} - 5^{th}$ Fresnel zones.

Multiple tags: We deployed more than one tag based on the optimization scheme presented in Section 4.2. From Fig. 20, we can see that by adding a second tag, the percentage of sensible zones was increased to 80% and 61% in the FFZ and $2^{nd} - 5^{th}$ Fresnel zones, respectively. We further increased the number of tags and measured the percentage of sensible zones. Fig. 20 shows that when the number of tags reached 5, "dead zone" in $1^{st} - 5^{th}$ Fresnel zones were completely removed (i.e., 0%). Note that when too many (e.g., more than ten) tags are deployed, each tag's reading rate will be decreased and thus, we suggest to deploy less than eight tags to work with a single reader.

5.2.3 Comparison to the Wi-Fi-based Respiration Sensing. To compare our "dead zone" removal method to the state-of-the-art Wi-Fi-based approach proposed in FullBreathe [52], we conducted experiments under the setup shown in Fig. 21 (a). For the Wi-Fi-based approach, we used the same deployment as introduced in FullBreathe [52]: the transmitter was equipped with one omni-directional antenna and the receiver was equipped with two omni-directional antennas. The packet was transmitted at the 5.745 GHz frequency band and the Channel State Information (CSI) was collected at a 100 Hz sampling rate. For RFID, we kept one directional antenna at the reader end. We chose a $1.5 \times 2 \ m^2$ size bed as our test area for both devices, which was divided into 100 grids. In each grid, the target was asked to lie on the bed and naturally breathe. The percentages of the sensible zones of the Wi-Fi-based approach vs. the proposed LungTrack are shown in Fig. 21 (b), which clearly demonstrates the superior sensing capability of LungTrack. More specifically, after combining the amplitude and phase information, LungTrack could achieve 80% of sensible zones, which was larger than that of FullBreath's coverage (65%). This was much expected since the amplitude and phase information in RFID are both more stable compared to Wi-Fi, as we discussed in Section 4.2. Furthermore, the remaining 20% of the bad or medium sensible zones of LungTrack were concentrated at the edges of the bed, where people rarely locate themselves during sleep in practice. The detection accuracy of this experiment was better than the results reported in Section 5.2.1, because of the difference in the equipment setup. In this experiment, the tags and reader were separated by 1.8 m and placed 30 cm above the bed. Hence, in most of the cases, the target chest is inside the FFZ.

5.2.4 Interference from Daily In-place Activities. In this experiment, we evaluated LungTrack's performance when the target was performing other daily activities, as shown in Fig. 22 (a)-(g), which we hypothesized to generate large signal interference.
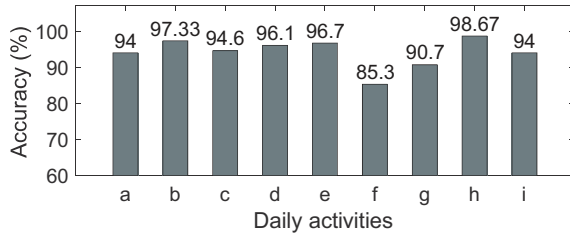
Fig. 22. Accuracy in presence of daily in-place activities (a-g) and other interfering persons (h-i). a: typing on a keyboard; b: playing a phone game; c: calling including picking up and answering the phone; d: walking (1.3 m/s); e: jogging (2.2 m/s); f: running (5 m/s); g: writhing the upper body; h: one interfering person walks around LoS; i: two interfering persons walk around LoS.
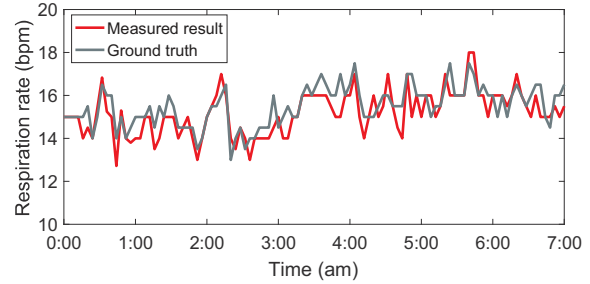

Fig. 23. Continuous respiration rate monitoring results. The figure shows that our system can achieve an average monitoring error of 0.55 bpm in the real sleep scenario.

Note that the target performed walking, jogging, and running on a treadmill. For each activity, the human target repeated the experiments ten times. In Fig. 22 (a)-(g), we can see that, except for high-speed running, LungTrack can achieve higher than 90% detection accuracy for various activities of daily living. We believe the inferior accuracy for high-speed running was caused by the movements of other body parts (e.g., arm swing) that shared a similar frequency as the respiration rate, interfering the detection algorithm.

The secondary objective of this experiment was to evaluate the robustness of the proposed system when other human subjects ambulate within the sensing range and create signal interference. Fig. 22 (h)-(i) shows the results. When another human subject walked around the target and introduced signal multipath and interference, the performance was not affected since the significant interference only occurred when the subject was very close to LoS (affected within only a short period of time).

5.2.5 Continuous Respiration Rate Monitoring. We also test our system in continuous monitoring scenario for one night (0 : 00 am − 7 : 00 am). In this experiment, the target slept naturally on a bed with the experimental setup shown in Fig. 18 (b). We recorded the ground-truth using a camera system with light on. The video showed that the target had a series of unconscious activities during sleep, including rolling his body, scratching his head, coughing, etc. Fig. 23 shows that with five RFID tags and our interference removal mechanism, we could accurately detect respiration and achieve an average monitoring error of 0.55 bpm (breath per minute) in this realistic sleeping scenario.

5.2.6 Multi-person Respiration Rate Monitoring. In this experiment, we evaluated the sensing performance when there were two targets in the sensing area. We considered a scenario for monitoring the respiration rates of two human targets sleeping on a bed. We recruited two random human targets and asked them to breathe naturally, lying on a queen-sized bed, as shown in Fig. 18 (c). One reader and two tags were deployed with the method described in Section 4.3. We evaluated our multi-target monitoring scheme with varying physical distances between the two targets. Fig. 24 summarizes the evaluation of the sensing accuracy. From the top figure, we can observe that, even when the two targets have very similar respiration rates (i.e.,the most challenging experimental scenario), our system could still achieve am accuracy higher than 99% (two targets were separated by 50 cm). The bottom figure shows that the sensing accuracy increases when the distance between the two targets increases. This is expected since the two tags' sensible zones would overlap if the two targets are placed very close to each other. When the two targets were separated by more than 20 cm, our system could achieve an accuracy higher than 95%.

5.2.7 Various Impact Factors. **Impact of anthropometric variation in human targets:** In this experiment, we evaluate LungTrack's respiration sensing performance in two human targets with different anthropometric characteristics (i.e., physical variation) in order to demonstrate 1) the limitations of utilizing a single RFID tag in respiration sensing and 2) the opportunities for the proposed method of minimizing "dead zones" using multiple tags. Target *A* (male) had a chest thicknesses of 27 cm and target *B* (male) had a chest thicknesses of 19 cm. The results at two typical locations are shown in Fig. 25. We can see
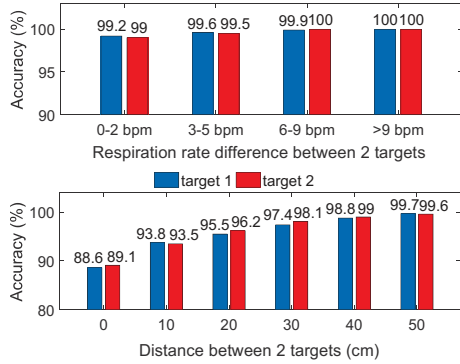
Fig. 24. Multi-target respiration monitoring. *The figure shows LungTrack's accuracy versus the 2 targets' respiration rate difference (top), and LungTrack's accuracy versus the two targets' distance (bottom).*
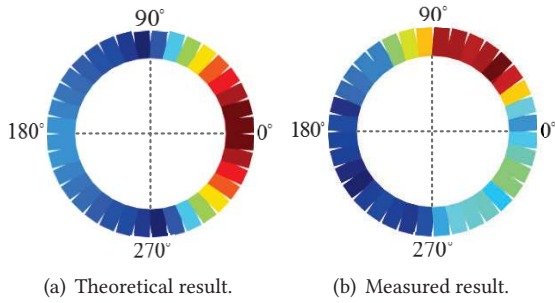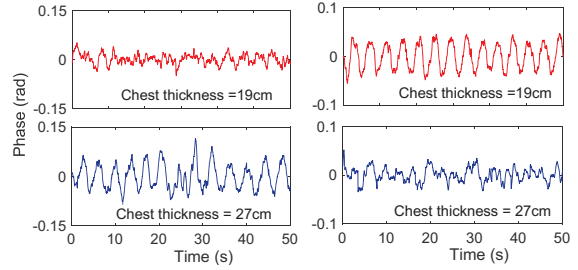

(a) Measurements at location 1.   (b) Measurements at location 2.

Fig. 25. Impact of anthropometric variation in human targets. *The figure shows that the good locations for targets with different chest thickness are very different.*

(a) Theoretical result.   (b) Measured result.

Fig. 26. Impact of human target orientation on the respiration rate detection accuracy in sitting scenario.

(a) Experimental setup.   (b) Measured results.

Fig. 27. Impact of the tag orientation. The figure shows the respiration sensing distance at the perpendicular bisector of LoS, in various tag orientations. The current tag orientation is $0°$.

that location 1, where $h = 5\ cm$ and $d_1 = d_2 = 75\ cm$ as in Fig. 2, has a good sensing performance for target A but a poor performance for target B. On the other hand, location 2, where $h = 12.5\ cm$, $d_1 = 50\ cm$, and $d_2 = 100\ cm$, showed good performance for target B but poor performance for target A. The primary reason for this phenomenon is that, during the process of respiration, the target's front as well as the back side of the chest show movements. When the two targets are located at the same location, the actual positions of the front chest and back are different due to different chest thicknesses. For example, if we align the front chest of the two targets at exactly the same position, then the back side of the chest showed a difference of 8 cm, which will cause a difference in sensing performance. Thus, a sensible zone for target A may not necessarily be a sensible zone for target B, mainly due to different antrophometric characteristics. This result also demonstrates the necessity of removing the "dead zones" to ensure good performance for any target at all the locations.

Impact of target orientation: In this experiment, a human target was asked to sit at the boundary of the FFZ bisecting the LoS perpendicularly. The target was facing the LoS initially and rotated the body from $0°$ to $360°$ at a step size of $10°$. The theoretical and experimental results are shown in Fig. 26, which clearly demonstrates some degree of discrepancies. One possible reason could be that for theoretical results, the target was assumed to be a point within the sensing region. In reality,

(a) Single target.

(b) Two targets.

Fig. 28. Impact of target sleep posture. It can be seen that LungTrack operates well in all of the above scenes except when targets are hugging each other.

the target had a non-negligible size and the size of the FFZ was also relatively small. Hence, when the target was rotating, the distance from the target to the transceivers also changed. In addition to the changes in the orientation, the changes in the distance also significantly affected the respiration sensing per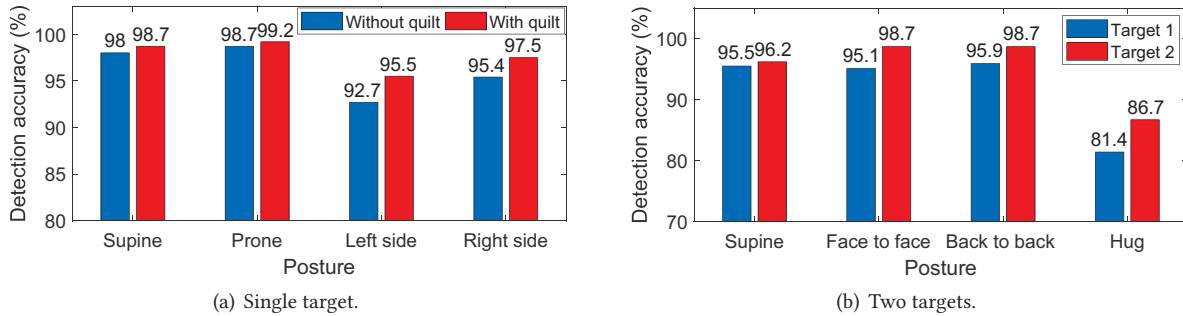formance. Furthermore, the directionality of the RFID antenna also conflicted with the symmetrical property of the theoretical results.

Impact of the tag orientation: We also investigated how the tag orientation affects the respiration sensing range. In this experiment, we asked the target to sit to perpendicularly bisect the LoS path and face the middle point of the LoS path. We rotated the tag as shown in Fig. 27 at a step size of $10°$. At each orientation of the tag, we measured the maximum sensing distance. The normalized distance information at each orientation is shown in Fig. 27. We can observe that the tag's orientation could affect the sensing capability, and there exist certain orientations that show good or poor sensing performance.

Impact of target sleep posture: In this experiment, we studied the impact of sleep postures on respiration rate monitoring in 1) single target and 2) two target scenarios. For the single target scenario. we considered four sleep postures: supination, pronation, facing left side, and facing right side. Fig. 21 (a) shows the experimental setup. Fig. 28 (a) shows the respiration rate detection accuracy resulted from different sleep postures. We could observe that our system can achieve greater than 92% of detection accuracy for all sleep postures, which demonstrates the robustness of our system for different realistic sleep postures. Another important observation includes that the accuracy resulted from the supination and pronation were greater than facing sideways. This is expected since the sensible body area (i.e., chest and back) and its displacement of the first two postures are larger than those of the last two postures (shoulders). We also tested our system's performance when target was covered with a quilt. The respiration rate detection accuracy presented in Fig. 28 (a) shows that our system could achieve better sensing performance when the target was covered with the quilt. We believe the primary reason for this interesting phenomenon is because the undulating surface of the quilt was larger than that of target body without the quilt during respiration.

We investigated four different postures for the experiment involving two targets: supination, face-to-face, back-to-back, and hug. Fig 18 (c) shows the experimental setup. The two targets were lying in bed while separated by 20 *cm* for the first three postures. Fig. 28 (b) shows that our system can achieve a detection accuracy of greater than 95% in the first three sleep postures. But when the two targets were hugging each other, the accuracy degrades substantially, because our proposed method was no longer capable of removing the mutual interference.

Impact of demographic and anthropometric variation: To evaluate the generalizability of our system's respiration rate detection accuracy in a larger population, we recruited ten human targets with various demographic and antrophometric characteristics, as summarized in Table 1. Each target was monitored for ten minutes. Fig. 29 shows the acquired average respiration rates of the ten targets and their ground truth. We achieved an accuracy of 98.7% for estimating respiration rate in adult and elder, but a lower accuracy of 88% for children due to their smaller breath depth (4 *mm*). More interestingly, when we compare Target 5 vs. Target 4 who show a large difference in the breath depth (i.e., 9 *mm* for Target 5 and 5 *mm* for

Table 1. Statistics of participant. The breath depth is obtained by laser range meter HILTI PD-I [9] that has the measurement accuracy of 1 *mm*.

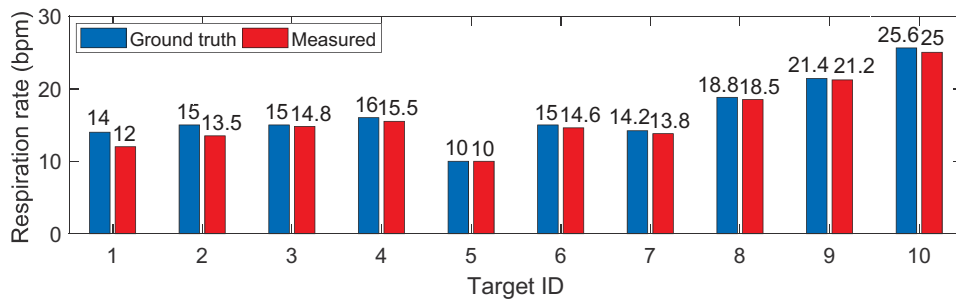| Target ID	1	2	3	4	5	6	7	8	9	10
Sex	Male	Male	Female	Female	Male	Female	Male	Female	Male	Female
Age	11	12	20	22	26	31	40	54	62	88
Height (*cm*)	130	141	158	160	185	165	172	160	178	146
Weight (*kg*)	31	35	53	49	85	57	68	60	78	48
Breath depth (*mm*)	4	4	6	5	9	6	7	7	8	7

Fig. 29. Respiration rate detection of diverse targets. The figure shows that our system can detect respiration rate with average accuracy of 98.7% for larger than 5 *mm* respiration depth.

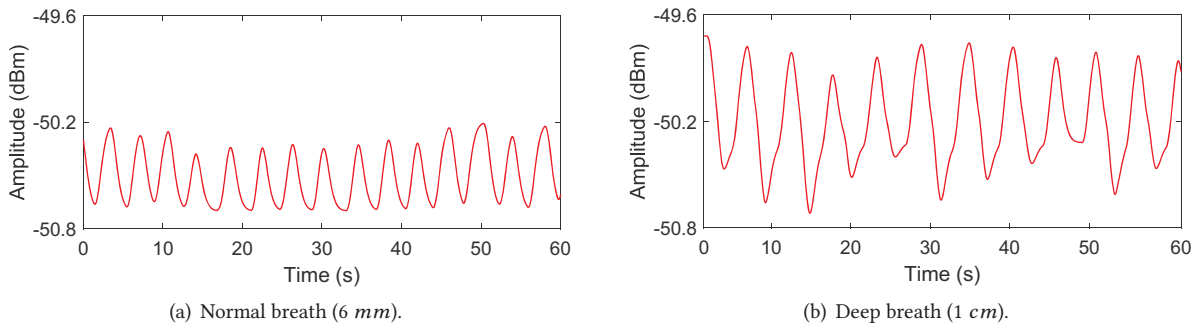(a) Normal breath (6 *mm*).

(b) Deep breath (1 *cm*).

Fig. 30. Signal changes caused by different depths of breath. It is obvious that the deep breath induces larger signal variation, thus the higher sensing accuracy.

Target 4), we can observe that the sensing accuracy for Target 5 is much higher due to more prominent chest movements during breathing. To visually explain the impact of the breath depth in the reflected signal changes, Fig. 30 shows a randomly selected target's (i.e., Target 6) normal breathing (6 *mm*) vs. deep breathing (10 *mm*), which clearly demonstrates the increase in the signal variations according to the breath depth. It is noteworthy that the respiration rates in elderly subjects (e.g., Target 9 and 10) were relatively higher than other subjects due to their smaller lung capacity.

6 DISCUSSION

Known target location range: LungTrack can minimize the "dead zones" in the single target scenario and avoid the mutual interference of multiple targets, both of which rely on *a priori* information regarding the locations of the target. Therefor, the proposed approaches herein are recommended for sleep or in-place activity scenarios, where location variation is minimal. Especially for the sleep monitoring application, the bed size is in line with the unified standard, so users will not need to calibrate the system by themselves again. In future work, we will continue to refine our approach to make the system suitable for a broader range of applications.

Use of a directional antenna for RFID reader: The use of a directional antenna can reduce the amount of multipaths in the indoor settings. However, it also reduces the sensing area of the system. Employing more than one directional antenna can be an option to cover the 360 degrees around the reader. The commodity R420 RFID reader together with the GIO hub supports a maximum of 16 antennas, which can be a promising direction for future studies.

Placement of human targets at a distance from the reader-tag pair: When the human target is placed distance away from the reader-tag pair (e.g., at the outer-most boundary of the Fresnel zones), the reflection signals may become too weak to be recognized for sensing. We believe that advanced signal processing techniques, such as JADE [25] and SAGE [50], could help us to retrieve relevant information from extremely weak signals and thus increase the sensing range.

7 RELATED WORK

LungTrack is related to the following categories of efforts in respiration sensing.

Device-based respiration monitoring: Polysomnography [33] and capnography are two standard clinical approaches for diagnosing respiration related health conditions in the medical setting. These methods, however, are costly and require a large number of sensors attached to the human subject during the monitoring process. While many portable monitoring systems [16, 17, 20, 39] have been proposed for use in home and community settings, these systems still require the attachment of multiple sensors on the body and, more importantly, require the presence of a trained technician to administrate the setup process [37].

Camera-based respiration monitoring: Advancement in image and signal processing enabled researchers to detect respiration by amplifying visual patterns recorded in video [21, 41, 46, 49]. By analyzing the color changes of a sequence of video images, researchers were able to extract information related to blood flow, and chest and abdominal movements caused by respiration. However, the camera-based approaches require the target to face the camera under a good light source.

Sound-based respiration monitoring: A number of studies have leveraged microphones on mobile and ubiquitous devices (e.g., smartphones) to monitor human respiration, which further enables the detection of the target's cough [24], snoring [3], and events related to sleep apnea [42]. A recent work by Ren *el al.* has leveraged audible breathing sounds from an ear bud to infer the breathing frequency [43]. An Android application, namely iBreath [23], combines the audible breathing sounds from a Bluetooth headset with the accelerometer on a smartphone to infer the breathing frequency while running.

Geophone-based respiration monitoring: Recently, the use of geophones to sense bed vibrations caused by ballistic force has shown great potential in monitoring a person's respiration during sleep [26, 27]. The geophone-based respiration monitoring systems hold the possibility of allowing user to move around and change position freely during sleep. While these system can only detect users lying in bed, the system's performance is limited to different postures such as sitting on a chair or standing.

Wireless-based respiration monitoring: The latest research has attempted to analyze RF signals for respiration monitoring. The most widely studied methods include Doppler radar [18, 38], UWB radar [36, 47], FMCW radar [14, 51, 54], and wireless sensor nodes [28, 40]. These systems could achieve high accuracy, while require a wide frequency band supported by dedicated and expensive hardware. Some commodity Wi-Fi systems [12, 31, 48, 53] have been proposed recently for respiration detection. However, these methods confine the target to sit or lie in a fixed location and the "dead zone" issue severely constraints their application in real-world scenarios. For example, a small movement of the target may cause the system to fail. The latest work [52] has leveraged the complementarity of amplitude and phase to address the "dead zone" problem in Wi-Fi. However, its ability to eliminate the "dead zones" is still limited since the phase information collected from commodity Wi-Fi devices is quite noisy. These Wi-Fi-based systems also have poor performance in multi-target scenarios due to the interference between the targets, especially when the targets breathe at a similar rate. Zhao *et al.* has verified the feasibility of using commodity

RFIDs for no-contact respiration monitoring [55], yet it still suffers from the "dead zones" and multi-target interference problems.

Compared to the above-mentioned prior work, LungTrack uses a commodity RFID reader and a number of low-cost RFID tags to achieve accurate device-free respiration sensing for the single target, as well as the multi-target, scenarios.

8 CONCLUSION

This paper presents LungTrack, a contactless respiration monitoring system built on commodity RFID hardware. Our system design is guided by the Fresnel diffraction and reflection theories, originally proposed for communication. With our proposed schemes, we successfully minimized the "dead zones" to facilitate accurate respiration sensing at most of the locations within the sensing range (within $1^{st} - 5^{th}$ Fresnel zones) for applications involving a single target. Furthermore, for applications involving multiple tagers, we have utilized the "dead zones" to attenuate the interference from the targets—a well-known problem for passive sensing—and enable simultaneous, accurate respiration sensing. Our comprehensive experiments also have demonstrated that our system could provide robust sensing performance during a number of activities of daily living, which could cause substantial signal interference. We believe our methods proposed in this work and the reported findings could provide new research opportunities for a large range of RFID-based, contactless sensing application, such as localization and activity recognition.

ACKNOWLEDGMENTS

REFERENCES

[1] Could a breath-monitoring headset improve your health? Website, 2013.
[2] Respiration: Single or dual-band. Website, 2013.
[3] Sleep as android: Snoring detection. Website, 2013.
[4] Alien. Website, 2015.
[5] Epcglobal epc gen2. Website, 2015.
[6] Finger pulse oximeter. Website, 2015.
[7] Impinj. Website, 2015.
[8] Rfmax s9028pcr antenna. Website, 2015.
[9] Hilti. Website, 2016.
[10] Sleep apnea: Epidemiology. Website, 2016.
[11] Dynamic time warping. Website, 2018.
[12] Heba Abdelnasser, Moustafa Youssef, and Moustafa Youssef. Ubibreathe: A ubiquitous non-invasive wifi-based breathing estimator. In *Proc. ACM (MobiHoc)*, 2015.
[13] Fadel Adib, Zachary Kabelac, Hongzi Mao, Dina Katabi, and Robert C. Miller. *Demo: real-time breath monitoring using wireless signals.* 2014.
[14] Fadel Adib, Hongzi Mao, Zachary Kabelac, Dina Katabi, and Robert C. Miller. Smart homes that monitor breathing and heart rate. In *Proc. ACM (CHI)*, 2015.
[15] J. A. Anderson and Vann Wf Jr. Respiratory monitoring during pediatric sedation: pulse oximetry and capnography. 1988.
[16] Guha Balakrishnan, Fredo Durand, and John Guttag. Detecting pulse from head motions in video. In *Proc. IEEE (CVPR)*, 2013.
[17] Jagmohan Chauhan, Yining Hu, Suranga Seneviratne, Archan Misra, Aruna Seneviratne, and Youngki Lee. Breathprint: Breathing acoustics-based user authentication. In *Proc. ACM (MobiSys)*, 2017.
[18] Y. F Chen, Devendra Misra, Huei Wang, and Huey Ru Chuang. An x-band microwave life-detection system. *Biomedical Engineering IEEE Transactions on*, 33(7):697–701, 1986.
[19] Halperin D, Hu W, Sheth A, and et al. Predictable 802.11 packet delivery from wireless channel measurements[j]. *ACM SIGCOMM Computer Communication Review*, 41(4):159–170, 2011.
[20] P. A. Deutsch, M. S. Simmons, and J. M. Wallace. Cost-effectiveness of split-night polysomnography and home studies in the evaluation of obstructive sleep apnea syndrome. *Journal of Clinical Sleep Medicine Jcsm Official Publication of the American Academy of Sleep Medicine*, 2(2):145–153, 2006.

[21] Jonathan E and Leahy M. Investigating a smartphone imaging unit for photoplethysmography. *Physiological measurement*, 31(11):79, 2010.
[22] H Gokalp and M Clarke. Monitoring activities of daily living of the elderly and the potential for its use in telecare and telehealth: a review. *Telemedicine journal and e-health : the official journal of the American Telemedicine Association*, 19(12):910, 2013.
[23] Tian Hao, Guoliang Xing, and Gang Zhou. ibreath: A convenient mobile app that tracks breathing during running.
[24] Tian Hao, Guoliang Xing, and Gang Zhou. isleep: Unobtrusive sleep quality monitoring using smartphones. In *Proc. ACM (SenSys)*, 2013.
[25] Shekh MM Islam, Ehsan Yavari, Ashikur Rahman, Victor M Lubecke, and Olga Boric-Lubecke. Separation of respiratory signatures for multiple subjects using independent component analysis with the jade algorithm. In *Proc.IEEE (EMBC)*, 2018.
[26] Zhenhua Jia and et al. Hb-phone: A bed-mounted geophone-based heartbeat monitoring system. In *Proc. IEEE (IPSN)*, 2017.
[27] Zhenhua Jia and et al. Monitoring a person's heart rate and respiratory rate on shared bed using geophones. In *Proc. ACM (SenSys)*, 2017.
[28] Kaltiokallio, Ossi Johannes, and Neal Patwari. Non-invasive respiration rate monitoring using a single cots tx-rx pair. In *In Proceedings of the International Symposium on Information Processing in Sensor Networks*, 2014.
[29] Qian Kun and et al. Pads: Passive detection of moving targets with dynamic speed using phy layer information. In *Proc. IEEE (ICPADS)*, 2014.
[30] Jian Liu, Yan Wang, Yingying Chen, Jie Yang, Xu Chen, and Jerry Cheng. Tracking vital signs during sleep leveraging off-the-shelf wifi. In *Proc. ACM (MobiHoc)*, 2015.
[31] Xuefeng Liu, Jiannong Cao, Shaojie Tang, and Jiaqi Wen. Wi-sleep: Contactless sleep monitoring via wifi signals. In *Proc. IEEE (RTSS)*, 2014.
[32] C. Lowanichkiattikul, M. Dhanachai, C. Sitathanee, S. Khachonkham, and P. Khaothong. Impact of chest wall motion caused by respiration in adjuvant radiotherapy for postoperative breast cancer patients. *Springerplus*, 5(1):144, 2016.
[33] J. F. Masa, J Corral, R Pereira, J Durancantolla, M Cabello, L Hernandezblasco, C Monasterio, A Alonso, E Chiner, and M Rubio. Effectiveness of home respiratory polygraphy for the diagnosis of sleep apnoea and hypopnoea syndrome. *Thorax*, 66(7):567–573, 2011.
[34] Marcel Miynczak and Gerard Cybulski. Improvement of body posture changes detection during ambulatory respiratory measurements using impedance pneumography signals. In *Mediterranean Conference on Medical and Biological Engineering and Computing*, 2004.
[35] Andreas F. Molisch. Wireless communications. *John Wiley and Sons*, 4(5):25–55, 2008.
[36] Phuc Nguyen, Xinyu Zhang, Ann Halbower, and Tam Vu. Continuous and fine-grained breathing volume monitoring from afar using wireless signals. In *Proc. IEEE (INFOCOM)*, 2016.
[37] M. B. Norman, S Middleton, O Erskine, P. G. Middleton, J. R. Wheatley, and C. E. Sullivan. Validation of the sonomat: a contactless monitoring system used for the diagnosis of sleep disordered breathing. *Sleep*, 37(9):1477–87, 2014.
[38] M. Nowogrodzki, DD. Mawhinney, and HF. Milgazo. Non-invasive microwave instruments for the measurement of respiration and heart rates. *NAECON*, 1984.
[39] R Paradiso. Wearable health care system for vital signs monitoring. In *International IEEE Embs Special Topic Conference on Information Technology Applications in Biomedicine*, 2004.
[40] Neal Patwari, Lara Brewer, Quinn Tate, Ossi Kaltiokallio, and Maurizio Bocca. Breathfinding: A wireless network that monitors and locates breathing in a home. *IEEE Journal of Selected Topics in Signal Processing*, 8(1):30–42, 2013.
[41] Jochen Penne, Christian Schaller, Joachim Hornegger, and Torsten Kuwert. Robust real-time 3d respiratory motion detection using time-of-flight cameras. *International Journal of Computer Assisted Radiology and Surgery*, 3(5):427–431, 2008.
[42] Nandakumar Rajalakshmi, Gollakota Shyamnath, and Nathaniel Watson M.D. Contactless sleep apnea detection on smartphones. In *Proc. ACM (MobiSys)*, 2015.
[43] Yanzh Ren, Chen Wang, Yingying Chen, and Jie Yang. Poster: Hearing your breathing: fine-grained sleep monitoring using smartphones. In *Proc. ACM (Mobicom)*, 2014.
[44] Longfei Shangguan and Kyle Jamieson. Leveraging electromagnetic polarization in a two-antenna whiteboard in the air. In *Proc. ACM (CoNEXT)*, 2016.
[45] R Steele, A Lo, C Secombe, and Y. K. Wong. Elderly persons' perception and acceptance of using wireless sensor networks to assist healthcare. *International Journal of Medical Informatics*, 78(12):788–801, 2009.
[46] K. S. Tan, R. Saatchi, H. Elphick, and D. Burke. Real-time vision based respiration monitoring system. *Proc. IEEE (CSNDSP)*, pages 770–774, 2010.
[47] S. Venkatesh, C. R. Anderson, N. V. Rivera, and R. M. Buehrer. Implementation and analysis of respiration-rate estimation using impulse-based uwb. In *Proc. IEEE (MILCOM)*, 2006.
[48] Hao Wang, Daqing Zhang, Junyi Ma, Yasha Wang, Yuxiang Wang, Dan Wu, Tao Gu, and Bing Xie. Human respiration detection with commodity wifi devices: do user location and body orientation matter? In *Proc. ACM (UbiComp)*, 2016.
[49] Haoyu Wu, Michael Rubinstein, Eugene Shih, John Guttag, Fredo Durand, and William Freeman. Eulerian video magnification for revealing subtle changes in the world. In *Proc. ACM (SIGGRAPH)*, 2012.
[50] Yaxiong Xie, Jie Xiong, Mo Li, and Jamieson Kyle. md-track: Leveraging multi-dimensionality inpassive indoor wi-fi tracking. In *Proc. ACM (Mobicom)*, 2018.

[51] Shichao Yue, Hao He, Hao Wang, Rahul Hariharan, and Katabi Dina. Extracting multi-person respiration from entangled rf signal signals. In *Proc. ACM (UbiComp)*, 2018.
[52] Youwei Zeng, Dan Wu, Ruiyang Gao Gao, Tao Gu, and Daqing Zhang. Fullbreathe: Full human respiration detection exploiting complementarity of csi phase and amplitude of wifi signals. In *Proc. ACM (UbiComp)*, 2018.
[53] Fusang Zhang, Daqing Zhang, Jie Xiong, Hao Wang, Kai Niu, Beihong Jin, and Yuxiang Wang. From fresnel diffraction model to fine-grained human respiration sensing with commodity wi-fi devices. In *Proc. ACM (UbiComp)*, 2018.
[54] Mingmin Zhao, Shichao Yue, Dina Katabi, Tommi Jaakkola, and Matt Bianchi. Learning sleep stages from radio signals: A conditional adversarial architecture. In *In International Conference on Machine Learning*, 2017.
[55] Run Zhao, Dong Wang, Qian Zhang, Haonan Chen, and Anna Huang. Crh: A contactless respiration and heartbeat monitoring system with cots rfid tag. In *Proc. IEEE (SECON)*, 2018.